machines

MDPI

Article

Motion Sickness Suppression Strategy Based on Dynamic Coordination Control of Active Suspension and ACC

Fang Zhou, Dengfeng Zhao, Yudong Zhong, Pengpeng Wang, Junjie Jiang, Zhenwei Wang and Zhijun Fu *

Henan Provincial Key Laboratory of Intelligent Manufacturing of Mechanical Equipment, Zhengzhou University of Light Industry, Zhengzhou 450002, China; 2020021@zzuli.edu.cn (F.Z.); zhaodf@zzuli.edu.cn (D.Z.); zhongyd@zzuli.edu.cn (Y.Z.); wpeng121@126.com (P.W.); jiangjunjie@zzuli.edu.cn (J.J.); 2024034@zzuli.edu.cn (Z.W.)

* Correspondence: fuzhijun2008@163.com

Abstract

With the development of electrification and intelligent technologies in vehicles, ride comfort issues represented by motion sickness have become a key constraint on the performance of autonomous driving. The occurrence of motion sickness is influenced by the comprehensive movement of the vehicle in the longitudinal, lateral, and vertical directions, involving ACC, LKA, active suspension, etc. Existing motion sickness control method focuses on optimizing the longitudinal, lateral, and vertical directions separately, or coordinating the optimization control of the longitudinal and lateral directions, while there is relatively little research on the coupling effect and coupled optimization of the longitudinal and vertical directions. This study proposes a coupled framework of ACC and active suspension control system based on MPC. By adding pitch angle changes caused by longitudinal acceleration to the suspension model, a coupled state equation of half-car vertical dynamics and ACC longitudinal dynamics is constructed to achieve integrated optimization of ACC and suspension for motion suppression. The suspension active forces and vehicle acceleration are regulated coordinately to optimize vehicle vertical, longitudinal, and pitch dynamics simultaneously. Simulation experiments show that compared to decoupled control of ACC and suspension, the integrated control framework can be more effective. The research results confirm that the dynamic coordination between the suspension and ACC system can effectively suppress the motion sickness, providing a new idea for solving the comfort conflict in the human vehicle environment coupling system.

Keywords: motion sickness suppression; model predictive control; half-car suspension system; adaptive cruise control; coordinated control

check for updates

Received: 10 June 2025
Revised: 10 July 2025
Accepted: 22 July 2025
Published: 24 July 2025

Citation: Zhou, F.; Zhao, D.; Zhong, Y.; Wang, P.; Jiang, J.; Wang, Z.; Fu, Z. Motion Sickness Suppression Strategy Based on Dynamic Coordination Control of Active Suspension and ACC. *Machines* **2025**, *13*, 650. https://doi.org/10.3390/machines13080650

Copyright: © 2025 by the authors. Licensee MDPI, Basel, Switzerland. This article is an open access article distributed under the terms and conditions of the Creative Commons Attribution (CC BY) license (https://creativecommons.org/licenses/by/4.0/).

1. Introduction

Motion sickness is a physiological functional disorder syndrome that occurs in specific motion environments, characterized by typical symptoms such as motion sickness, nausea, vomiting, and cold sweats. Its underlying mechanism stems from neural compensatory imbalance triggered by perceptual conflicts among the vestibular, visual, and proprioceptive systems [1]. With the accelerated transformation of the automotive industry toward the "new four modernizations", L2 and above-intelligent EVs have become core components of urban intelligent transportation systems [2]. However, this shift has been accompanied by a significant increase in the incidence of in-vehicle motion sickness, which compromises the comfort of transportation experiences [3].

From the perspective of vehicle dynamics, the longitudinal and vertical dynamic characteristics of EVs are key factors aggravating motion sickness. The high torque and rapid response of electric motors, combined with electro-mechanical braking, result in nonlinear fluctuations during acceleration/deceleration, suspension vibrations induced by road excitation reduce ride comfort, the coupling effect between suspension vibrations and longitudinal dynamic induces pitch motion, significantly increasing motion sickness risk [4]. Autonomous driving tends to cause sensory conflict between visual and vestibular systems, thereby increasing the likelihood of motion sickness occurrence [5].

Thus, against the backdrop of electrification and intelligentization, motion sickness-related ride comfort has emerged as a critical issue that cannot be overlooked. There is an urgent need to incorporate motion sickness mitigation metrics into vehicle control systems. Current research on motion sickness in intelligent EVs primarily focuses on two aspects: motion sickness prediction and motion sickness suppression control. Research on motion sickness prediction can be further divided into intrinsic physiological mechanisms of motion sickness and the correlation between vehicle motion parameters and motion sickness incidence.

In the study of intrinsic physiological mechanisms of motion sickness, Keshavarz et al. [6] systematically summarized the physiological mechanisms of neural compensatory imbalance, while Laessoe et al. [7] and Ng et al. [8] demonstrated the regulatory effect of visuo-vestibular synchronization on symptoms. Gruden et al. [9] further validated through EGG that such conflicts directly translate into quantifiable physiological signals. Studies also identified significant individual variability in susceptibility, with motion sickness-prone individuals exhibiting higher sensitivity to perceptual mismatches [10,11].

In the study of the relationship between vehicle motion parameters and motion sickness, longitudinal, lateral, and vertical accelerations are found to significantly correlate with motion sickness [12]. Zhao et al. [13] established a prediction model using vehicle accelerations through driving tests, and Tian et al. [14] further added trip duration and individual variability in the model to improve prediction accuracy. Iskander et al. [15] specifically investigated non-driving-related activities in autonomous vehicles, developing a predictive framework for such scenarios. Kia et al. [16] experimentally verified that active suspension seats could reduce WBV and corresponding motion sickness. Jin et al. [17] demonstrate that semi-active suspension can effectively alleviate motion sickness by suppressing vertical acceleration and pitch angular velocity.

Based on the foregoing analysis, motion sickness primarily stems from two physiological mechanisms: sensory conflict between visual and vestibular inputs and the impact of vehicle motion states. Critical vehicle-induced motion sickness parameters include vertical acceleration at the center of mass, pitch angular velocity, and longitudinal acceleration, all of which demonstrate strong correlations with motion sickness incidence.

In the field of motion sickness suppression control, researchers have achieved preliminary results in both vehicle dynamics optimization and intelligent motion planning algorithms.

Cui et al. [18] proposed an adaptive wheelbase preview robust H_∞ control method that can accurately identify road roughness information and suppress vehicle body vibration. It not only satisfies driving smoothness but also takes into account passenger driving experience. Chen et al. [19] proposed an intelligent chassis-coordinated control algorithm that combines wheel ground tangential force control that effectively improves the vertical vibration acceleration level of the body, reduces the incidence rate of motion sickness, and improves the driving comfort and other comprehensive performance of intelligent chassis vehicles. Feng et al. [20] proposes a model predictive control-based integrated torque vectoring and active suspension strategy, optimizing longitudinal and vertical dynamics

via a linear time-varying half-vehicle model, effectively enhancing energy efficiency and ride comfort of four-wheel independently driven electric vehicles while ensuring stability. Liang et al. [21] proposed a decentralized cooperative control framework of AFS and ASS by applying MDMPC, effectively enhancing the vehicle lateral and vertical stability during path tracking. Zheng et al. [22] propose a nonlinear model predictive control method for curve tilt function for active suspension in vehicle lateral motion to counteract inertial lateral acceleration. The lateral acceleration is significantly reduced to suppress the occurrence of motion sickness. Winkel et al. [23] demonstrate that discomfort increases with acceleration and jerk and propose a motion comfort prediction model.

In motion planning, researchers have developed various comfort-oriented trajectory planning methods. Htike et al. [24] and Geng et al. [25] achieved a balance among motion sickness reduction, driving safety, and driving efficiency through multi-objective optimization. Li et al. [26] developed a motion-planning algorithm incorporating frequency-shaping techniques and significantly reduced MSDV compared to conventional methods. Rajesh et al. [27] applied DRL to autonomous vehicle trajectory planning to minimize low-frequency accelerations and thereby suppress motion sickness symptoms. Additionally, Gysen et al. [28] and Papaioannou et al. [29] investigated the structure and performance of active suspension systems, demonstrating their effectiveness in mitigating motion sickness.

Although the aforementioned studies have achieved significant progress in vehicle dynamics control and intelligent motion planning, most results have focused on longitudinal–lateral cooperative control and steady-state lateral–vertical control during steering maneuvers. Research on the coupling mechanisms and cooperative control of vertical–longitudinal excitations, which significantly influence motion sickness, remains insufficient. The longitudinal acceleration changes generated by ACC systems during car-following or speed adjustments can aggravate vehicle pitch motion, acting on the front and rear suspensions. Traditional suspension control primarily targets the suppression of road-induced vibrations transmitted through tires, often lacking coordinated optimization for ACC-induced pitch motion or merely treating speed/acceleration as disturbances to the controller, resulting in suboptimal performance. Moreover, current ACC algorithms mainly focus on safety and fuel efficiency, paying less attention to the impact of acceleration/deceleration profiles on passenger comfort. Meanwhile, suspension control often overlooks the interference of longitudinal vehicle motion on body posture. Such fragmented control strategies make it difficult to fundamentally address motion sickness. Therefore, the coordinated control of ACC and suspension systems is crucial for motion sickness suppression. By integrating ACC acceleration planning with active suspension control and incorporating both suspension control forces and longitudinal vehicle acceleration as control variables, it is possible to optimize body pitch and vertical vibration characteristics during acceleration/braking. This approach enables coordinated longitudinal–vertical dynamics coupling control, effectively suppressing the occurrence of motion sickness.

Based on the above analysis, this study focuses on motion sickness suppression control technologies for autonomous vehicles. The main approach involves coupled modeling and control of active suspension and ACC to coordinately regulate longitudinal and vertical dynamics and suppress motion sickness. The paper is structured as follows: Section 2 presents coupled dynamic modeling of the suspension and ACC systems along with control system design; Section 3 provides simulation verification; and Section 4 offers conclusions and future perspectives.

2. Materials and Methods

2.1. Vertical Dynamics

In this study, the vehicle's pitch motion induced by front and rear suspension interactions is identified as one of the contributing factors to motion sickness. Half-car suspension model is introduced to characterize this feature. This model integrates two quarter-car suspensions; model construction is shown in Figure 1.

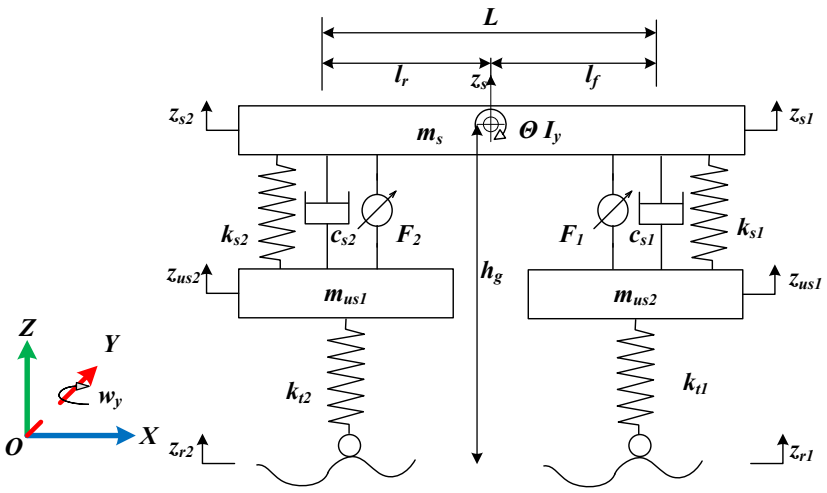


Figure 1. Half-car suspension model.

In Figure 1, m_s is the sprung mass, m_{us1} and m_{us2} represent the unsprung masses of the front and rear suspensions, respectively, F_{s1} and F_{s2} represent the spring forces of the front and rear suspensions, k_{s1} and k_{s2} represent the spring stiffnesses of the front and rear suspensions, F_{d1} and F_{d2} represent the damping forces of the front and rear suspensions, c_{s1} and c_{s2} represent their respective damping coefficients, F_1 and F_2 represent the active control forces of the front and rear suspensions, F_{t1} and F_{t2} represent the elastic forces generated by the front and rear tires, k_{t1} and k_{t2} represent the equivalent spring stiffnesses of the front and rear tires, z_s represents the vertical displacement of the sprung mass center, z_{s1} and z_{s2} represent the vertical displacements at the connection points between the sprung mass and the front/rear suspensions, z_{us1} and z_{us2} represent the vertical displacements of the front and rear unsprung mass centers, z_{r1} and z_{r2} represent the vertical road excitations acting on the front and rear tires, I_y represents the moment of inertia of the sprung mass about the Y-axis, and θ represents the pitch angle. The combined action of the front and rear suspensions induces variations in the pitch angle, with displacements and forces defined as positive in the upward direction.

Based on the vertical force balance analysis, the vertical dynamics equation of the sprung mass m_s is:

$$m_s\ddot{z}_s = F_{s1} + F_{d1} + F_{s2} + F_{d2} + F_1 + F_2 \tag{1}$$

In which:

$$F_{s1} = -k_{s1}(z_{s1} - z_{us1}) \tag{2}$$

$$F_{d1} = -c_{s1}(\dot{z}_{s1} - \dot{z}_{us1}) \tag{3}$$

$$F_{s2} = -k_{s2}(z_{s2} - z_{us2}) \tag{4}$$

$$F_{d2} = -c_{s2}(\dot{z}_{s2} - \dot{z}_{us2}) \tag{5}$$

Based on the geometric kinematics of the sprung mass pitching:

$$z_{s1} = z_s - l_f sin\theta \tag{6}$$

$$z_{s2} = z_s + l_r sin\theta \tag{7}$$

Based on the moment balance analysis about the Y-axis, the pitch dynamics equation of the sprung mass m_s is:

$$I_y\ddot{\theta}_s = -l_f(F_{s1} + F_{d1} + F_1) + l_r(F_{s2} + F_{d21} + F_2) \tag{8}$$

The vertical dynamics equation for the front unsprung mass m_{us1} is derived as:

$$m_{us1}\ddot{z}_{s1} = -F_{s1} - F_{d1} - F_1 + F_{t1} \tag{9}$$

$$F_{t1} = -k_{t1}(z_{us1} - z_{ur1}) \tag{10}$$

The vertical dynamics equation for the rear unsprung mass m_{us2} is derived as:

$$m_{us2}\ddot{z}_{s2} = -F_{s2} - F_{d2} - F_2 + F_{t2} \tag{11}$$

$$F_{t2} = -k_{t2}(z_{us2} - z_{ur2}) \tag{12}$$

Furthermore, since vehicle acceleration/deceleration induces pitch motion and affects front/rear suspension dynamics, the disturbance input from longitudinal acceleration a_{ego} is incorporated into the half-car suspension model. During acceleration/deceleration, ground reaction forces generate a pitch moment about the Y-axis at the center of mass. This moment is added to the equations to characterize the coupling effect of a_{ego} on suspension dynamics. Consequently, Equation (8) is modified as:

$$I_y\ddot{\theta}_s = -l_f(F_{s1} + F_{d1} + F_1) + l_r(F_{s2} + F_{d21} + F_2) - m_s a_{ego} h_g \tag{13}$$

In which, a_{ego} represents ego car acceleration, h_g is sprung mass center of gravity height.

Based on the above analysis, a control-oriented model for the half-car suspension system is constructed as follows:

Model Control Variables: $U_{sus} = [F_1, F_2]^T$

Model Disturbance Inputs: $U_{dsus} = [z_{r1}, z_{r2}, a_{ege}]^T$

Model State Variables: $X_{sus} = [z_s, \theta, z_{us1}, z_{us2}, \dot{z}_s, \dot{\theta}, \dot{z}_{us1}, \dot{z}_{us2}]$

Model Output Variables: $Y_{sus} = [\dot{z}_s, \theta, z_{s1} - z_{us1}, z_{s2} - z_{us2}]$

System model is

$$\begin{cases} \dot{X}_{sus} = A_{sus}X_{sus} + B_{sus}U_{sus} + B_{dsus}U_{dsus} \\ Y_{sus} = C_{sus}X_{sus} \end{cases} \tag{14}$$

Based on the model above, system matrix A_{sus}, B_{sus}, B_{dsus}, and C_{sus} are represented as:

$$A_{sus} = \begin{pmatrix} 0 & 0 & 0 & 0 & 1 & 0 & 0 & 0 \\ 0 & 0 & 0 & 0 & 0 & 1 & 0 & 0 \\ 0 & 0 & 0 & 0 & 0 & 0 & 1 & 0 \\ 0 & 0 & 0 & 0 & 0 & 0 & 0 & 1 \\ -\frac{k_{s1}+k_{s2}}{m_s} & \frac{k_{s1}l_f - k_{s2}l_r}{m_s} & \frac{k_{s1}}{m_s} & \frac{k_{s12}}{m_s} & -\frac{c_{s1}+c_{s2}}{m_s} & \frac{c_{s1}l_f - c_{s2}l_r}{m_s} & \frac{c_{s1}}{m_s} & \frac{c_{s2}}{m_s} \\ \frac{k_{s1}l_f - k_{s2}l_r}{I_y} & -\frac{k_{s1}l_f^2 + k_{s2}l_r^2}{I_y} & -\frac{k_{s1}l_f}{I_y} & \frac{k_{s2}l_r}{I_y} & \frac{c_{s1}l_f - c_{s2}l_r}{I_y} & -\frac{c_{s1}l_f^2 + c_{s2}l_r^2}{I_y} & -\frac{c_{s1}l_f}{I_y} & \frac{c_{s2}l_r}{I_y} \\ \frac{k_{s1}}{m_{s1}} & -\frac{k_{s1}l_f}{m_{s1}} & -\frac{k_{s1}+k_{r1}}{m_{s1}} & 0 & \frac{c_{s1}}{m_{s1}} & -\frac{c_{s1}l_f}{m_{s1}} & -\frac{c_{s1}}{m_{s1}} & 0 \\ \frac{k_{s2}}{m_{s2}} & -\frac{k_{s2}l_r}{m_{s2}} & 0 & -\frac{k_{s2}+k_{r2}}{m_{s2}} & \frac{c_{s2}}{m_{s2}} & -\frac{c_{s2}l_r}{m_{s2}} & 0 & -\frac{c_{s2}}{m_{s2}} \end{pmatrix}_{8\times 8} \tag{15}$$

$$B_{sus} = \begin{pmatrix} 0 & 0 \\ 0 & 0 \\ 0 & 0 \\ 0 & 0 \\ \frac{1}{m_{s1}} & \frac{1}{m_{s1}} \\ \frac{l_f}{I_y} & -\frac{l_r}{I_y} \\ -\frac{1}{m_{s1}} & 0 \\ 0 & -\frac{1}{m_{s2}} \end{pmatrix}_{8\times 2} \quad B_{dsus} = \begin{pmatrix} 0 & 0 & 0 \\ 0 & 0 & 0 \\ 0 & 0 & 0 \\ 0 & 0 & 0 \\ 0 & 0 & 0 \\ 0 & 0 & -\frac{m_s h_g}{I_y} \\ \frac{k_{r1}}{m_{s1}} & 0 & 0 \\ 0 & \frac{k_{r2}}{m_{s2}} & 0 \end{pmatrix}_{8\times 3} \tag{16}$$

$$C_{sus} = \begin{pmatrix} 0 & 0 & 0 & 0 & 1 & 0 & 0 & 0 \\ 0 & 1 & 0 & 0 & 0 & 0 & 0 & 0 \\ 1 & -l_f & -1 & 0 & 0 & 0 & 0 & 0 \\ 1 & l_r & 0 & -1 & 0 & 0 & 0 & 0 \end{pmatrix}_{4\times 8} \tag{17}$$

2.2. ACC Control

ACC is a L2 ADAS. It calculates target acceleration and executes control based on information such as set speed, preceding vehicle speed, and relative distance. Typically, ACC is implemented using MPC. Below is a generic MPC-based ACC control methodology.

The ACC working principle is shown in Figure 2.

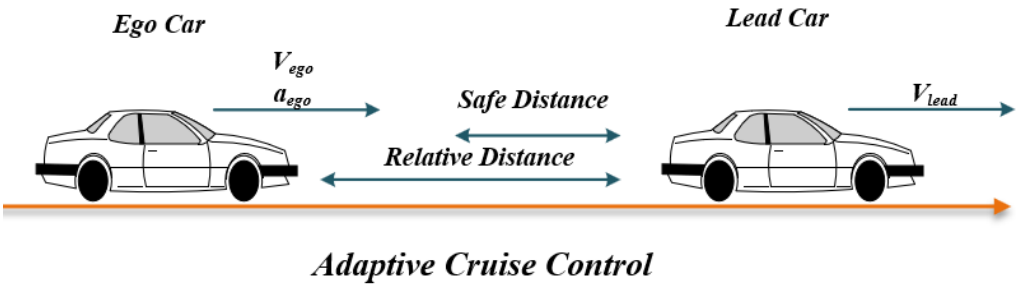


Figure 2. ACC principle.

In Figure 2, v_{lead} represents lead car velocity, d represents the distance between lead car and ego car, v_{ego} represents ego car velocity, and a_{ego} represents ego car acceleration. According to the vehicle motion equation, it can be concluded that:

$$\dot{d} = -v_{ego} + v_{lead} \tag{18}$$

$$\dot{v}_{ego} = a_{ego} \tag{19}$$

For vehicles, the execution of acceleration and deceleration signals requires passing through the actuator, introducing a time delay. Therefore, the target acceleration a_{cmd} is defined, and a first-order delay is assumed between a_{cmd} and a_{ego}:

$$\dot{a}_{ego} = \frac{1}{\tau}(a_{cmd} - a_{ego}) \tag{20}$$

In Equation (20), τ represents the actuator time constant. In this study, the EV actuator comprises the drive motor and other potential transmission mechanisms, and τ is selected as 0.2 s to represent the dynamic characteristics of them.

The control model of ACC is defined as follows:

Model Control Variables: $U_{acc} = a_{cmd}$

Model Disturbance Inputs: $U_{dacc} = v_{lead}$

Model State Variables: $X_{acc} = [d, v_{ego}, a_{ego}]^T$

Model Output Variables: $Y_{acc} = [d, v_{ego}, a_{ego}]^T$

According to the model above, system matrix is:

$$A_{acc} = \begin{pmatrix} 0 & -1 & 0 \\ 0 & 0 & 1 \\ 0 & 0 & -\frac{1}{\tau} \end{pmatrix}_{3\times3}, B_{acc} = \begin{pmatrix} 0 \\ 0 \\ \frac{1}{\tau} \end{pmatrix}_{3\times1}, B_{dacc} = \begin{pmatrix} 1 \\ 0 \\ 0 \end{pmatrix}_{3\times1}$$
$$C_{acc} = \begin{pmatrix} 1 & 0 & 0 \\ 0 & 1 & 0 \\ 0 & 0 & 1 \end{pmatrix}_{3\times3}, D_{acc} = [] \quad (21)$$

2.3. Coupled Dynamics Integration

The suspension control model described by Equations (14)–(17) is integrated with the ACC control model represented by Equation (21). During this integration process, a_{ego} transitions from an external disturbance to a controllable state variable.

Model Control Variables: $U = [F_1, F_2, a_{cmd}]^T$

Model Disturbance Inputs: $U_d = [z_{r1}, z_{r2}, v_{lead}]^T$

Model State Variables: $X = [z_s, \theta, z_{us1}, z_{us2}, \dot{z}_s, \dot{\theta}, \dot{z}_{us1}, \dot{z}_{us2}, d, v_{ego}, a_{ego}]$

Model Output Variables: $Y = [\dot{z}_s, \theta, z_{s1} - z_{us1}, z_{s2} - z_{us2}, d, v_{ego}, a_{ego}]$

The integrated matrix A is represented as:

$$A = \begin{pmatrix} A_{sus} & A_{acc\to sus} \\ A_{sus\to acc} & A_{acc} \end{pmatrix}_{11\times11} \quad (22)$$

Matrix $A_{acc\to sus}$ has dimensions of 8 × 3, representing the direct influence of the 3 variables in X_{acc} on the 8 variables in X_{sus}; in X_{acc} = [d, v_{ego}, a_{ego}], d and v_{ego} do not have any direct effect on X_{sus}, so the first two columns of $A_{acc\to sus}$ are entirely 0; only a_{ego} exerts a direct influence on a_{ego}. As a_{ego} corresponds to the third component of the disturbance vector B_{dsus} in the suspension control model, its mathematical relationship with X_{sus} is represented by the third column of B_{dsus}. Therefore, the third column of $A_{acc\to sus}$ is identical to the third column of B_{dsus}, $A_{acc\to sus}$ = [$0_{8\times2}$, B_{dsus}(:,3)].

Matrix $A_{sus\to acc}$ has dimensions of 3 × 8, representing the direct influence of the 8 variables in X_{sus} on the 3 variables in X_{acc}. However, since X_{sus} does not directly affect X_{acc}, $A_{sus\to acc}$ is a zero matrix.

Matrix A is represented as:

$$A = \begin{pmatrix} A_{sus} & [0_{8\times2}, B_{dsus}(:,3)] \\ 0_{3\times8} & A_{acc} \end{pmatrix}_{11\times11} \quad (23)$$

The integrated disturbance matrix B_{dsus} characterizes the direct influence of external disturbances U_d = [z_{r1}, z_{r2}, v_{lead}] on state vector X_{sus}.

Since a_{ego} from U_{dsus} has been converted to a state variable, its corresponding column in B_{dsus} has been transferred to the state matrix A. Consequently, B_{dsus} now retains only the first two columns, representing the direct effects of z_{r1} and z_{r2} on the system states.

Matrix B_d can be expressed as:

$$B_d = \begin{pmatrix} B_{dsus}(:,1:2) & 0_{8\times1} \\ 0_{3\times2} & B_{dacc} \end{pmatrix}_{11\times3} \quad (24)$$

In Equation (24), $0_{8\times1}$ indicates that v_{lead} does not directly disturb X_{sus}, while $0_{3\times2}$ indicates that z_{r1} and z_{r2} do not directly disturb X_{acc}.

Matrix B and C are integrated using a similar approach, and the final integrated system matrix is expressed as:

$$\begin{aligned} A &= \begin{pmatrix} A_{sus} & [0_{8\times2}, B_{dsus}(:,3)] \\ 0_{3\times8} & A_{acc} \end{pmatrix}_{11\times11}, B = \begin{pmatrix} B_{sus} & 0_{8\times1} \\ 0_{3\times2} & B_{acc} \end{pmatrix}_{11\times3}, \\ B_d &= \begin{pmatrix} B_{dsus}(:,1:2) & 0_{8\times1} \\ 0_{3\times2} & B_{dacc} \end{pmatrix}_{11\times3}, C = \begin{pmatrix} C_{sus} & 0_{4\times3} \\ 0_{3\times8} & C_{acc} \end{pmatrix}_{7\times11} \end{aligned} \tag{25}$$

2.4. MPC-Based Integrated Controller Design

MPC is a modern control theory based on receding horizon optimization and feedback correction. Its core principle involves constructing and solving finite-horizon optimization problems online, converting the optimization into a QP problem, as is shown in Figure 3. It computes the optimal control sequence for MIMO systems and dynamically applies this sequence to achieve real-time system regulation. In the context of motion sickness mitigation, MPC can reconcile conflicting objectives between suspension vertical forces and ACC longitudinal acceleration while handling system constraints.

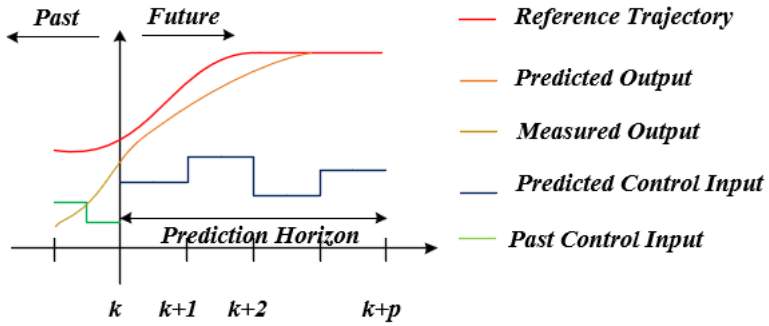


Figure 3. MPC principle.

MPC predicts future system dynamics based on a discretized state-space model. For the integrated half-vehicle suspension and ACC coupled system, the state equation can be formulated as:

$$\begin{cases} \dot{X} = AX + BU + B_d U_d \\ Y = CX \end{cases} \tag{26}$$

At each time step k, MPC generates a control sequence by solving the following optimization problem:

$$min \sum_{i=0}^{N_p-1} (\left|\left|y(k+i|k) - y_{ref}(k+i|k)\right|\right|_Q^2 + \left|\left|u(k+i|k)\right|\right|_R^2) + \rho\varepsilon^2 \tag{27}$$

After determining hyperparameters, weighting factors, and constraint parameters, the MPC algorithm transforms the control problem into a standard QP formulation as follows:

$$min \frac{1}{2}\Delta U^T H \Delta U + f^T \Delta U \tag{28}$$

where $\Delta U = [\Delta u(k|k), \Delta u(k+1|k), \ldots, \Delta u(k+N_c-1|k)]^T$ represents the control increment sequence applied to the system.

3. Results

3.1. Coupled Control System Architecture

The vehicle dynamics model and MPC-based control system incorporating both vertical and longitudinal motions was developed in Matlab/Simulink (R2024b). The model consists of two main components: the plant and the control system, as illustrated in Figure 4. The control system receives measured signals Y and noise U_d from the plant, estimates system states, solves the MPC optimization problem to derive control signals U, and finally applies them to the plant for closed-loop control.

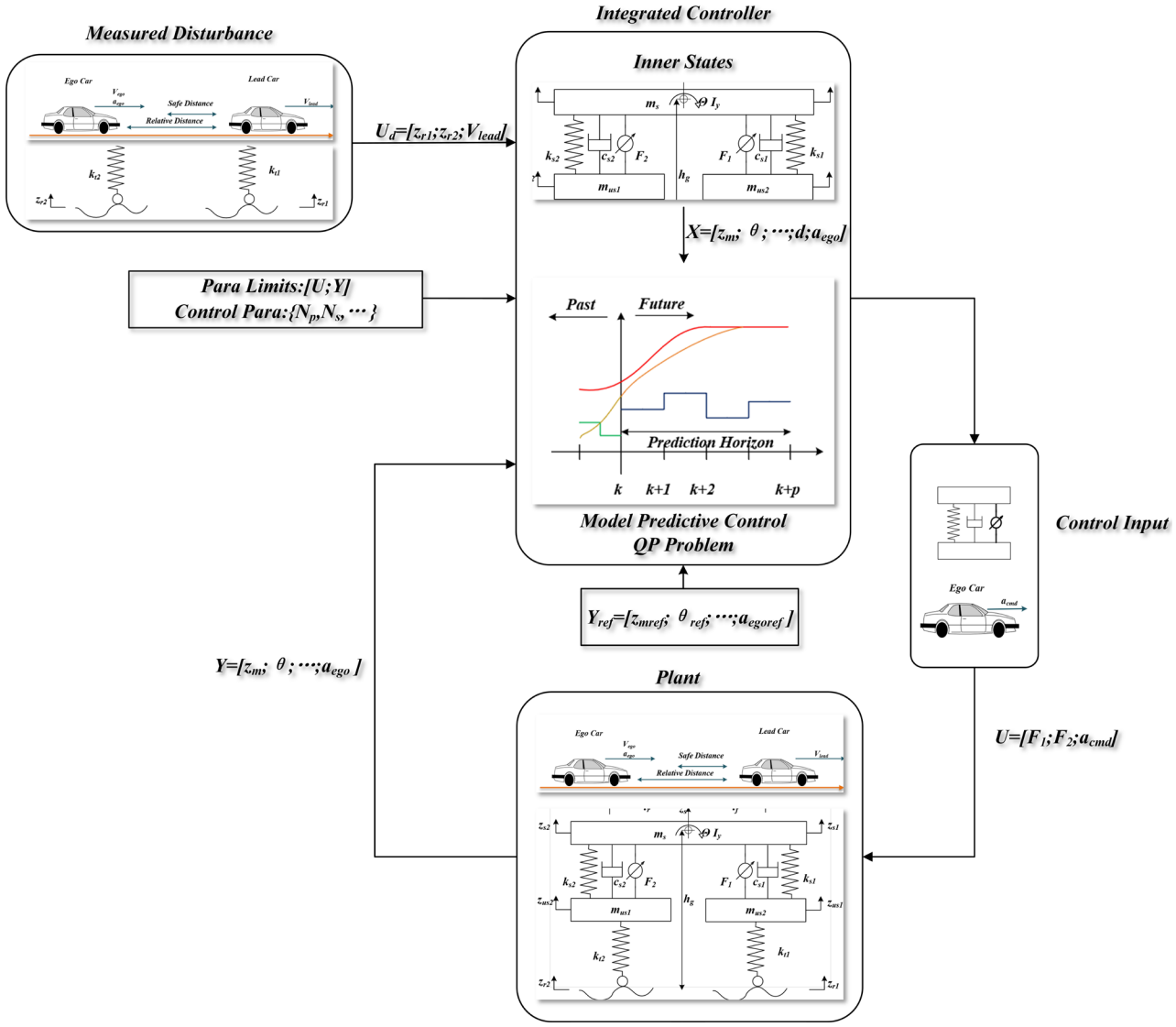


Figure 4. Integrated control architecture.

Vehicle parameters are detailed in Table 1.

Table 1. Parameters of the vehicle.

Parameter	Value
ms	1200 kg
Iy	1500 kg·m^2
mus1	40 kg
mus1	45 kg

Table 1. *Cont.*

Parameter	Value
ks1	25,000 N/m
ks2	27,000 N/m
cs1	1500 N·s/m
cs2	1600 N·s/m
kt1	200,000 N/m
kt2	210,000 N/m
lf	1.2 m
lr	1.5 m
hg	0.5 m

The designed MPC control system hyperparameters are listed in Table 2. The discretization period was determined by integrating suspension control and ACC requirements: while ACC typically operates at around 100 ms control cycles, suspension control requires shorter cycles of 5–20 ms to respond to high-frequency road excitations. Balancing ACC/suspension control demands and system complexity, a 20 ms control period was selected.

Table 2. MPC parameters.

Hyperparameter	Value
Discretization Period	0.02 s
Prediction Horizon	30
Control Horizon	20

The constructed controller is a linear MPC. According to the hyperparameter analysis in Table 2 and the control model architecture in Equation (25), the dimension of the Hessian matrix is 60 × 60, with a computational complexity of approximately O(60^3). It can stably run on automotive controllers and meet the real-time update requirement of 20 ms.

The control system's input/output constraints are listed in Table 3.

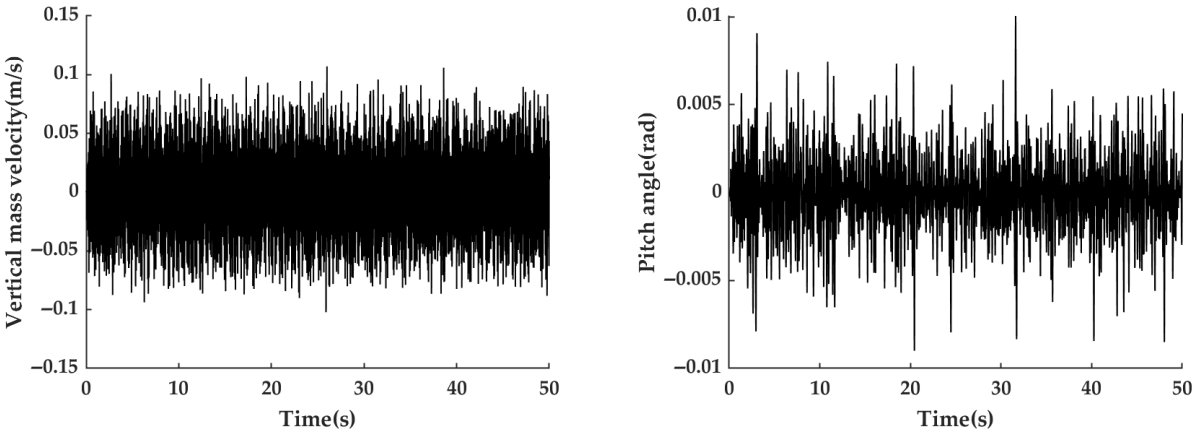
Table 3. Input/output constraints.

Parameter	Min.	Max.
F_1	−2000 N	2000 N
F_2	2000 N	2000 N
a_{cmd}	−5 m/s^2	5 m/s^2
$\dot{z}_s$	−0.3 m/s	0.3 m/s
θ	−8·π/180 rad	8·π/180 rad
$\dot{\theta}$	−3·π/180 rad/s	3·π/180 rad/s
$z_{s1} - z_{us1}$	−0.1 m	0.1 m
$z_{s2} - z_{us2}$	−0.1 m	0.1 m
d	50 m	250 m
v_{ego}	0 m/s	50 m/s
a_{ego}	−5 m/s^2	5 m/s^2

3.2. System Decoupled Simulation

3.2.1. Suspension Control Simulation

Based on the half-car suspension described in Section 2.1, simulation is conducted without considering disturbances from ACC. Suspension simulation is performed on a Class B road surface, with the results shown in Figure 5. It can be observed that the vertical velocity of the sprung mass is constrained within 0.1, and the pitch angle does not exceed 0.01 rad. These results demonstrate the multi-objective coordination capability of MPC.



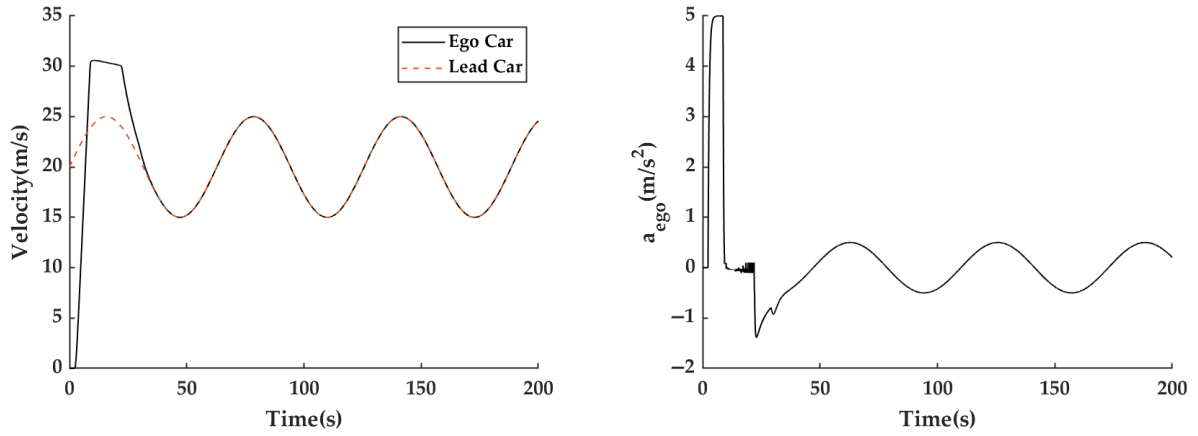
(**a**) (**b**)

Figure 5. Suspension control simulation: (**a**) sprung mass vertical velocity; (**b**) sprung mass pitch angle.

3.2.2. ACC Simulation

The ACC simulation is conducted using the MPC parameters listed in Table 2, with engineering constraints provided in Table 3.

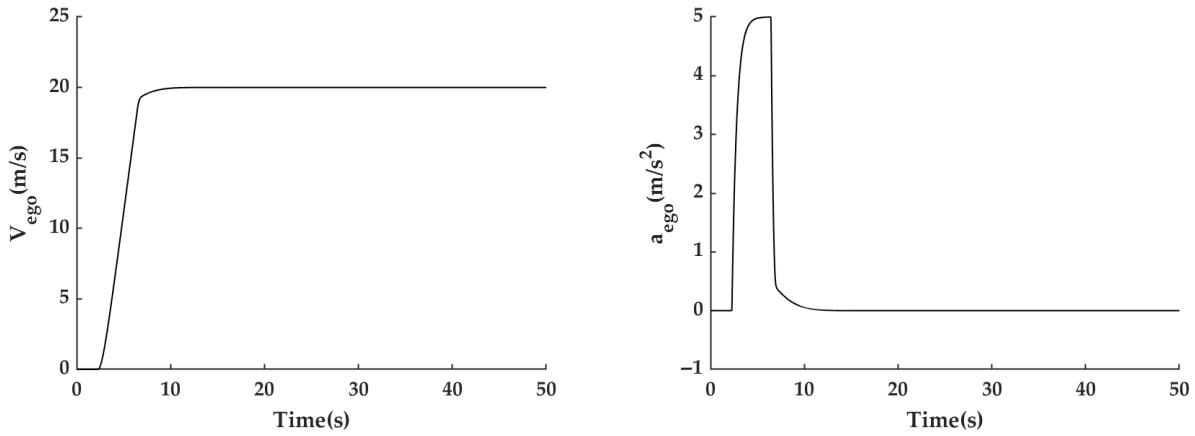
First, a following scenario is simulated. The lead car traveled at a sinusoidal speed, while the ego car starts from an initial speed of 0 m/s with a desired speed of 30 m/s. The simulation results are shown in Figure 6. It can be observed that the lead car speed significantly affects the ego car acceleration, which undoubtedly further influences the vertical dynamic characteristics.



(**a**) (**b**)

Figure 6. Car-following simulation: (**a**) velocity comparison of ego car and lead car; (**b**) acceleration of ego car.

Then, the cruise with constant velocity simulation is conducted with the target speed set at 20 m/s. As shown in Figure 7, the controller effectively tracks the target speed and rapidly converges to 20 m/s, and the acceleration remains strictly within predefined constraints.



(**a**) (**b**)

Figure 7. Constant speed simulation: (**a**) velocity of ego car; (**b**) acceleration of ego car.

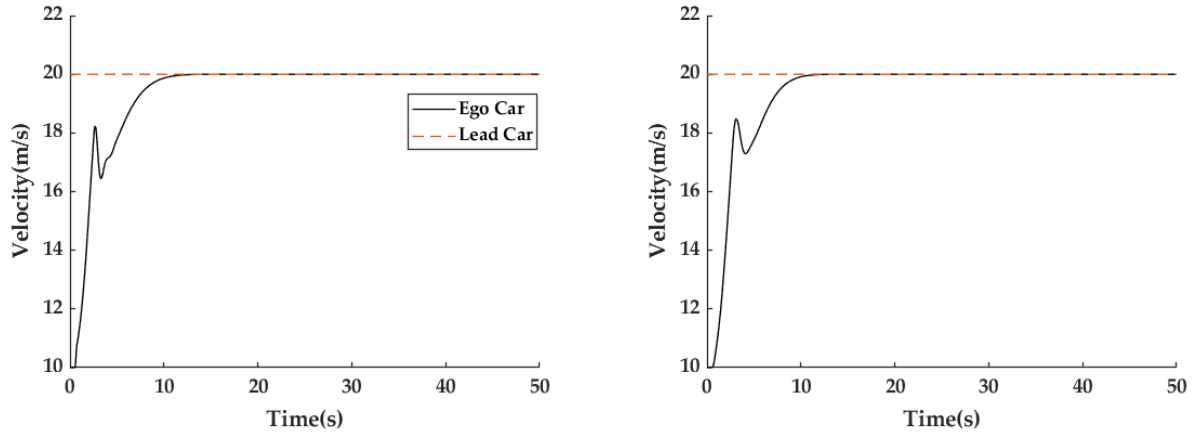
3.3. System Integrated Simulation

In conventional vehicle control architectures, ACC and suspension control systems typically operate in isolation. Therefore, this study first simulates such a decoupled control scheme as a baseline for comparison. Under this architecture, the acceleration computed by the ACC is treated as an external disturbance to the suspension control system, and suspension control performance does not feedback to influence the ACC acceleration.

In contrast, in the proposed control framework, the acceleration command of the ACC serves as a control variable in the integrated controller, introducing coupling with suspension dynamics, optimization of suspension performance consequently affects the vehicle's acceleration.

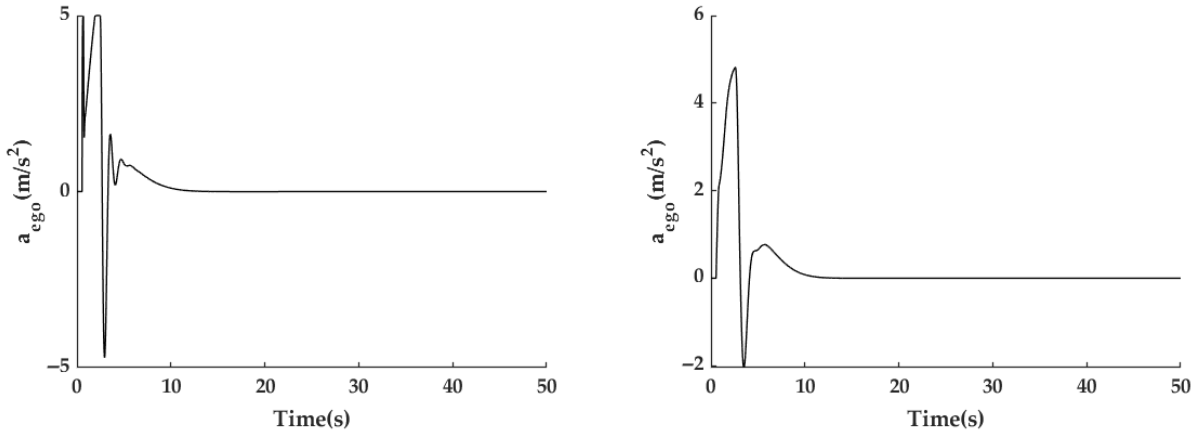
A simulation is conducted under steady-state following conditions: lead car velocity is 20 m/s; initial distance between lead car and ego car is 100 m; ego car initial velocity is 10 m/s; both front and rear suspensions are subjected to Class B road excitation.

As evident from Figures 8–11, the proposed integrated control strategy demonstrates significant improvements over decoupled control, longitudinal acceleration is effectively reduced, vertical velocity amplitude decreased at most time, pitch angle peak value reduced from 0.06 rad to 0.02 rad, and vehicle pitch dynamics caused by acceleration are effectively suppressed.



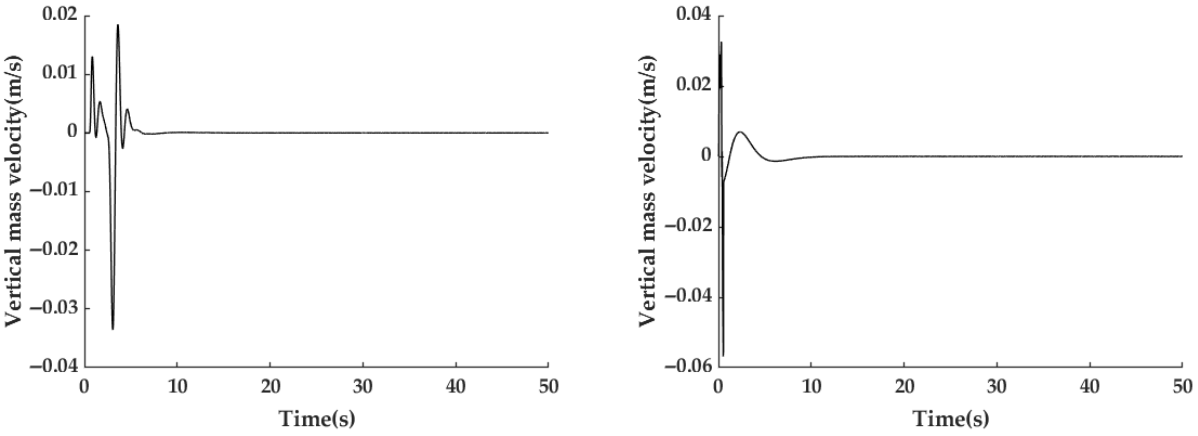
(**a**) (**b**)

Figure 8. Comparison of ego car velocity: (**a**) decoupled control; (**b**) proposed control.



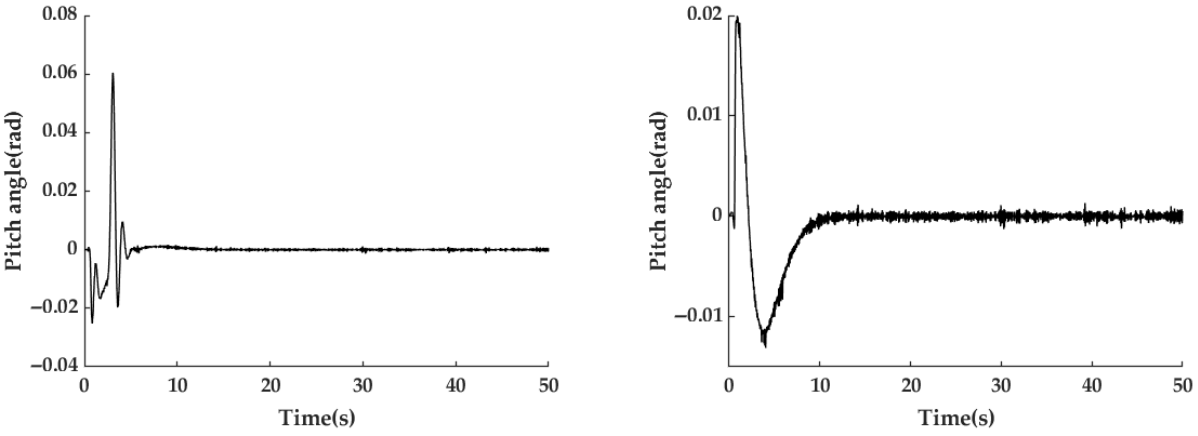
(**a**) (**b**)

Figure 9. Comparison of ego car acceleration: (**a**) decoupled control; (**b**) proposed control.



(**a**) (**b**)

Figure 10. Comparison of ego car sprung mass vertical velocity: (**a**) decoupled control; (**b**) proposed control.



(**a**) (**b**)

Figure 11. Comparison of ego car pitch angle: (**a**) decoupled control; (**b**) proposed control.

A simulation is conducted under car-following conditions: lead car velocity is a sinusoidal waveform with amplitude of 5 m/s, offset of 30 m/s, and frequency of 0.5 Hz; ego car initial velocity is 10 m/s, target velocity is 30 m/s, distance between lead car and ego car is 100 m, and both front and rear suspensions are subjected to Class B road

excitation. As evidenced in Figures 12–15, the proposed controller reliably maintains core ACC objectives under complex car-following conditions, specifically lead car tracking. Figure 13 demonstrates concurrent optimization of acceleration characteristics, in which the acceleration transition is smoother, and peak values are reduced. In Figures 14 and 15, both vertical velocity and pitch angle are much smaller and smoother than decoupled control, and the disturbance induced by the lead car sinusoidal acceleration is nearly eliminated, achieving near-zero convergence within 10 s after initial oscillations, demonstrating marked superiority. The proposed control strategy demonstrates significant improvements over conventional decoupled control, consequently achieving effective mitigation of motion sickness.

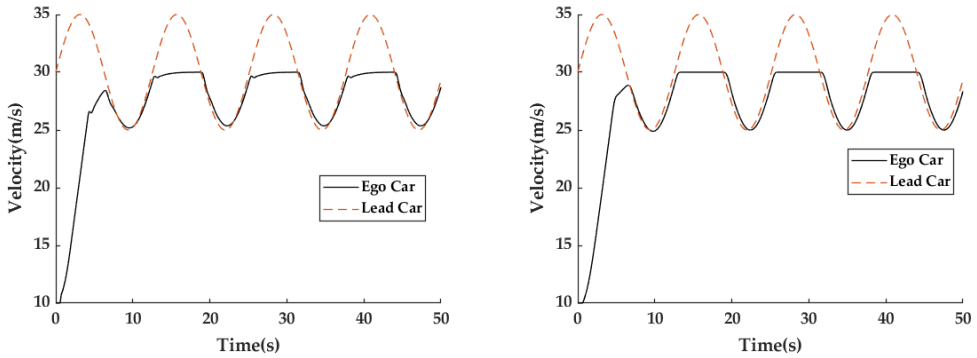


Figure 12. Comparison of velocity: (**a**) decoupled control; (**b**) proposed control.

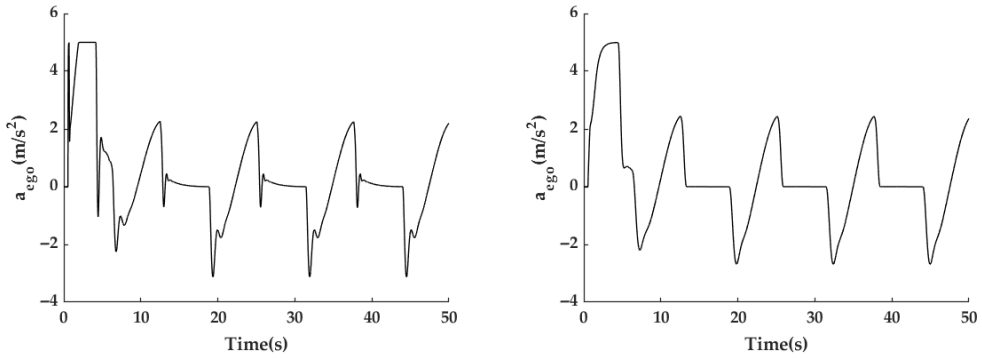


Figure 13. Comparison of acceleration: (**a**) decoupled control; (**b**) proposed control.

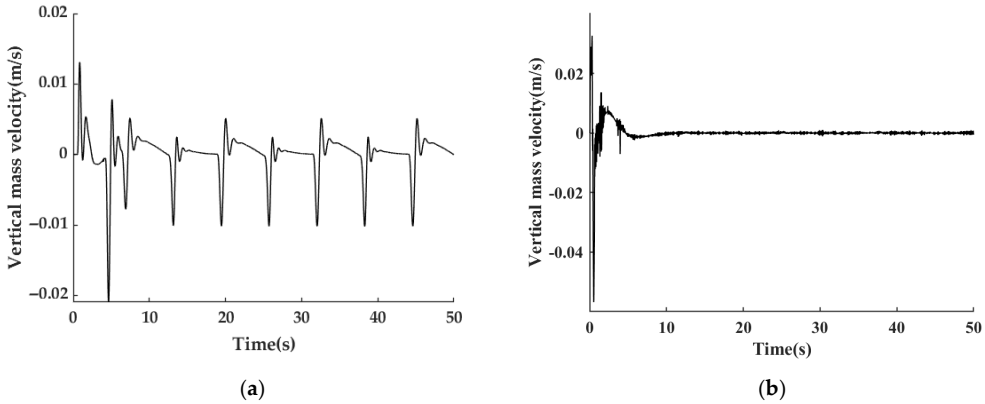
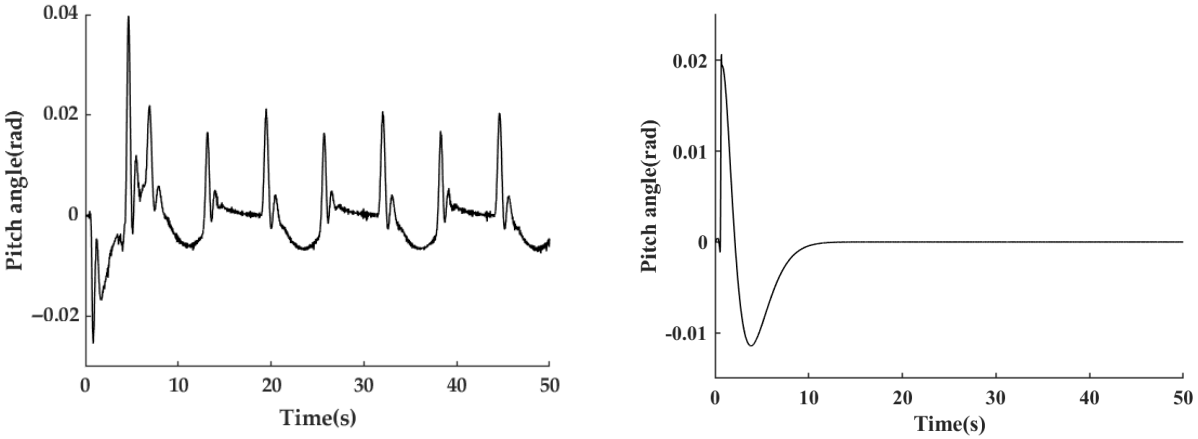


Figure 14. Comparison of sprung mass vertical velocity: (**a**) decoupled control; (**b**) proposed control.



(**a**) (**b**)

Figure 15. Comparison of pitch angle: (**a**) decoupled control; (**b**) proposed control.

RMS and MSDV of corresponding signals are calculated and compared, listing in Table 4. In Table 4, *jerk* describes the rate of change of vehicle acceleration over time and directly reflects the smoothness of acceleration variation. Excessive jerk can easily trigger passenger motion sickness, and w_y is pitch angular velocity. MSDV is calculated based on the ISO 2631-1 standard [30].

Table 4. RMS and MSDV comparison.

Driving Condition	Parameter	Method	RMS	MSDV
V_{lead}: *constant*	a_{ego}	decoupled	0.936	/
		coupled	0.846	/
	jerk	decoupled	4.18	/
		coupled	1.39	/
	θ_y	decoupled	0.0057	/
		coupled	0.0036	/
	v_{sz}	decoupled	0.0032	0.0295
		coupled	0.0033	0.1696
	w_y	decoupled	0.03	/
		coupled	0.018	/
V_{lead}: *sinusoidal*	a_{ego}	decoupled	1.72	/
		coupled	1.68	/
	jerk	decoupled	4.4	/
		coupled	1.72	/
	θ_y	decoupled	0.0068	/
		coupled	0.0035	/
	v_{sz}	decoupled	0.0031	0.0255
		coupled	0.0038	0.1721
	w_y	decoupled	0.0296	/
		coupled	0.0176	/

RMS of parameter a_{ego} and *jerk* of the proposed method are obviously smaller than those of the decoupled method, especially jerk, and the proposed method can effectively regulate longitudinal dynamics and suppresses motion sickness-related parameters.

RMS of parameter Θ_y and w_y are also significantly lower than those of decoupled control, indicating that the pitch motion induced by longitudinal acceleration has been effectively suppressed, thereby reducing the likelihood of motion sickness.

Parameter v_{sz} exhibits counterintuitive data trends—both RMS and MSDV values of the proposed method are higher than those of the decoupled method. However, as

shown in Figures 14 and 15, this increase primarily stems from a rapid, large-magnitude signal fluctuation during the very initial control phase. This transient spike results in significantly higher short-term acceleration variations in the MSDV calculation, leading to an inflated MSDV value. Notably, such fluctuations occur only once at startup. From a long-term control perspective, the proposed method still demonstrates exceptionally superior performance.

4. Conclusions

This article proposes a vertical and longitudinal coupling control for vehicles, including active suspension control and ACC. The suspension control system is designed based on a half-car model, and the pitch dynamics of the sprung mass induced by acceleration are also incorporated into the model. In ACC design, acceleration command is one of the control variables optimizing ACC and suspension-related objectives. The coupled control system is designed based on MPC: three control inputs are active control forces of front and rear suspension, and longitudinal acceleration; eleven states are eight suspension states and three ACC states. The target outputs mainly focus on three variables related to motion sickness: vertical velocity and pitch angle of the sprung mass, and longitudinal acceleration of the vehicle. By designing a coupled controller, the acceleration can be adjusted during the suspension control process to suppress pitch motion and optimize the suspension control effect.

The simulation compares the conventional suspension and ACC decoupled control with the proposed coupled method. The results demonstrate that (1) longitudinal acceleration will affect the suspension control effect, thereby exacerbating the parameters related to motion sickness; (2) the proposed coupling controller can optimize suspension control performance by adjusting acceleration while meeting the original objectives of ACC, thereby suppressing motion sickness-related parameters. The proposed method explores the performance of multi-dimensional coupling control of the chassis in terms of motion-related comfort and provides a feasible solution.

However, there are still some limitations to this study: (1) The nonlinear characteristics of the active suspension actuator have not been taken into account, which have a significant impact on suspension performance. Neglecting these factors may result in poor performance of the controller under actual operating conditions, especially under large-amplitude or high-frequency excitations, where the dynamic response of the suspension deviates significantly from the theoretical model, thereby affecting vehicle comfort and stability. (2) This study focuses on vehicle dynamics performance indicators, while motion sickness-related physiological signals (e.g., passenger head acceleration, EEG and visual–vestibular conflict) were not directly included in the optimization objectives, this may result in the control system improving mechanical performance but failing to effectively alleviate passenger motion issues. (3) Motion sickness is caused by the coupled effects of longitudinal, lateral, and vertical dynamics, and may have a cumulative effect; this study mainly focuses on longitudinal–vertical coupling dynamics, ignoring the lateral dynamics and cumulative effect of signals, which may result in inaccurate control effect in real driving conditions.

In future research, we will focus on the following aspects: (1) integrate the nonlinear actuator model into the control system to improve model accuracy; (2) develop a human mechanical model and establish the mathematical relationship between physiological indicators and control signals, directly using acceleration and other signals to regulate comfort metrics, achieving human–vehicle closed-loop control; (3) investigate longitudinal–lateral–vertical coupling control methods and identify the feasible spatial domain of

control inputs to simultaneously manage three-dimensional dynamics, thus mitigating motion sickness.

Author Contributions: Conceptualization, F.Z.; methodology, D.Z.; software, Y.Z.; validation, F.Z. and Y.Z.; formal analysis, J.J.; investigation, P.W.; resources, Z.F.; writing—original draft preparation, F.Z.; writing—review and editing, Z.W.; funding acquisition, Z.F. All authors have read and agreed to the published version of the manuscript.

Funding: This research was funded by Henan Natural Science Fund for Distinguished Young Scholars, grant number 252300421015, National Natural Science Foundation of China (NSFC), grant number 52472441, and Henan Center for Outstanding Overseas Scientists, grant number GZS2023011, Major Science and Technology Projects in Henan Province, grant number 241100240300, Henan Provincial Science and Technology Tackling Project, grant number 252102220101, Natural Science Foundation in Henan province of China, grant Number 242300421468.

Data Availability Statement: The dataset used in this research is available upon request by emailing the corresponding author.

Conflicts of Interest: The authors declare no conflicts of interest.

Abbreviations

The following abbreviations are used in this manuscript:

EVs	Electric Vehicles
AVs	Autonomous Vehicles
VR	Virtual Reality
EGG	Electrogastrography
EEG	Electroencephaogram
AFS	Active Front Steering
ASS	Active-suspension System
MDMPC	Multi-constrained Distributed Model Predictive Control
SSQ	Simulator Sickness Questionnaire
MSI	Motion Sickness Incidence
MSDV	Motion Sickness Dose Value
EDA	Electrodermal activity
WBV	Whole-body Vibration
LMI	Linear Matrix Inequality
MOGA	Multi-objective Genetic Algorithm
DRL	Deep Reinforcement Learning
ADAS	Advanced Driving Assistance System
MPC	Model Predictive Control
QP	Quadratic Programming
MIMO	Multiple-Input Multiple-Output

References

1. Diels, C.; Ye, Y.; Bos, J.E.; Maeda, S. Motion Sickness in Automated Vehicles: Principal Research Questions and the Need for Common Protocols. *SAE Int. J. Connect. Autom. Veh.* **2022**, *5*, 121–134. [CrossRef]
2. Li, Z.H.; Khajepour, A.; Song, J.C. A comprehensive review of the key technologies for pure electric vehicles. *Energy* **2019**, *182*, 824–839. [CrossRef]
3. Zheng, Y.G.; Shyrokau, B.; Keviczky, T. Mitigating Motion Sickness With Optimization-Based Motion Planning. *IEEE Trans. Intell. Veh.* **2024**, *9*, 2553–2563. [CrossRef]
4. Shi, Z.S.; He, L.; Wang, M.W.; Bian, Y.J.; Cui, S.H.; Chen, P.P. Ideal comfort ellipses and comfort dynamics model for mitigating motion sickness in battery electric vehicle. In *Vehicle System Dynamics*; Taylor & Francis: Abingdon, UK, 2024.
5. Asua, E.; Gutiérrez-Zaballa, J.; Mata-Carballeira, O.; Ruiz, J.A.; del Campo, I. Analysis of the Motion Sickness and the Lack of Comfort in Car Passengers. *Appl. Sci.* **2022**, *12*, 3717. [CrossRef]

6. Keshavarz, B.; Golding, J.F. Motion sickness: Current concepts and management. *Curr. Opin. Neurol.* **2022**, *35*, 107–112. [CrossRef] [PubMed]
7. Laessoe, U.; Abrahamsen, S.; Zepernick, S.; Raunsbaek, A.; Stensen, C. Motion sickness and cybersickness—Sensory mismatch. *Physiol. Behav.* **2023**, *258*, 114015. [CrossRef] [PubMed]
8. Ng, A.K.T.; Chan, L.K.Y.; Lau, H.Y.K. A study of cybersickness and sensory conflict theory using a motion-coupled virtual reality system. *Displays* **2020**, *61*, 101922. [CrossRef]
9. Gruden, T.; Popovic, N.B.; Stojmenova, K.; Jakus, G.; Miljkovic, N.; Tomazic, S.; Sodnik, J. Electrogastrography in Autonomous Vehicles-An Objective Method for Assessment of Motion Sickness in Simulated Driving Environments. *Sensors* **2021**, *21*, 550. [CrossRef]
10. Huang, J.; Liu, X.Z.; Hu, L. Review of Motion Sickness-associated Comfort Studies for Occupants in Autonomous Vehicles. *China J. Highw. Transp.* **2024**, *37*, 356–369.
11. Brietzke, A.; Xuan, R.P.; Dettmann, A.; Bullinger, A.C. Influence of dynamic stimulation, visual perception and individual susceptibility to car sickness during controlled stop-and-go driving. *Forsch. Ingenieurwes* **2022**, *12*, 3717. [CrossRef]
12. Deng, Z.X.; Yuan, K.; Xiao, X. Investigative examination of motion sickness indicators for electric vehicles. *Proc. Inst. Mech. Eng. Part D J. Automob. Eng.* **2025**, *239*, 3347–3357. [CrossRef]
13. Zhao, S.E.; Tian, Z.S.; Wei, H.b.B.; Xiao, X.; Wang, K.; Zeng, J. Evaluation Model of Passenger Motion Sickness Based on Vehicle Motion Parameters. *China J. Highw. Transp.* **2025**, *38*, 274–285.
14. Tian, Z.S.; Zhao, S.E.; Xiao, X.; Wei, H.B.; Wang, K.; Zeng, J. Evaluation of intelligent electric vehicle carsickness performance considering passenger motion sensitivity. *Proc. Inst. Mech. Eng. Part D J. Automob. Eng.* **2025**.
15. Iskander, J.; Attia, M.; Saleh, K.; Nahavandi, D.; Abobakr, A.; Mohamed, S.; Asadi, H.; Khosravi, A.; Lim, C.P.; Hossny, M. From car sickness to autonomous car sickness: A review. *Transp. Res. Part F Traffic Psychol. Behav.* **2019**, *62*, 716–726. [CrossRef]
16. Kia, K.; Johnson, P.W.; Kim, J.H. The effects of different seat suspension types on occupants? physiologic responses and task performance: Implications for autonomous and conventional vehicles. *Appl. Ergon.* **2021**, *93*, 103380. [CrossRef] [PubMed]
17. Jin, S.; Lee, C.; Rhee, E.; Jung, J.; Lee, C. Analysis of the Effects of Motion Sickness According to Damping Characteristics of Suspension. *Int. J. Auto. Technol.* **2025**, *26*, 991–999. [CrossRef]
18. Cui, M.; Fu, Z.J.; Rakheja, S.; Zhen, R.; Liu, Y.G. Adaptive Preview H$_\infty$ Control of Active Suspension Based on Road Recognition. *Automot. Eng.* **2025**, *47*, 508–518.
19. Chen, X.K.; Wang, H.Y.; Liu, H.Y.; Liu, X. Research on Coordinated Control of Semi-active Suspension of Intelligent Chassis and Ground Tangential Force. *J. Mech. Eng.* **2024**, *60*, 1–10.
20. Feng, J.W.; Liang, J.H.; Lu, Y.B.; Zhuang, W.C.; Pi, D.W.; Yin, G.D.; Xu, L.W.; Peng, P.; Zhou, C.B. An Integrated Control Framework for Torque Vectoring and Active Suspension System. *Chin. J. Mech. Eng.* **2024**, *37*, 10. [CrossRef]
21. Liang, J.H.; Lu, Y.B.; Pi, D.W.; Yin, G.D.; Zhuang, W.C.; Wang, F.A.; Feng, J.W.; Zhou, C.B. A Decentralized Cooperative Control Framework for Active Steering and Active Suspension: Multi-Agent Approach. *IEEE Trans. Transp. Electrif.* **2022**, *8*, 1414–1429. [CrossRef]
22. Zheng, Y.G.; Shyrokau, B.; Keviczky, T.; Al Sakka, M.; Dhaens, M. Curve Tilting with Nonlinear Model Predictive Control for Enhancing Motion Comfort. *IEEE Trans. Control Syst. Technol.* **2022**, *30*, 1538–1549. [CrossRef]
23. Winkel, K.N.D.; Irmak, T.; Happee, R.; Shyrokau, B. Standards for passenger comfort in automated vehicles: Acceleration and jerk. *Appl. Ergon.* **2023**, *106*, 103881. [CrossRef]
24. Htike, Z.; Papaioannou, G.; Siampis, E.; Velenis, E.; Longo, S. Fundamentals of Motion Planning for Mitigating Motion Sickness in Automated Vehicles. *IEEE Trans. Veh. Technol.* **2022**, *71*, 2375–2384. [CrossRef]
25. Geng, G.Q.; Wu, Z.; Jiang, H.B.; Sun, L.Q.; Duan, C. Study on Path Planning Method for Imitating the Lane-Changing Operation of Excellent Drivers. *Appl. Sci.* **2018**, *8*, 814. [CrossRef]
26. Li, D.F.; Hu, J.K. Mitigating Motion Sickness in Automated Vehicles with Frequency-Shaping Approach to Motion Planning. *IEEE Robot. Autom. Lett.* **2021**, *6*, 7714–7720. [CrossRef]
27. Rajesh, N.; Zheng, Y.G.; Shyrokau, B. Comfort-Oriented Motion Planning for Automated Vehicles Using Deep Reinforcement Learning. *IEEE Open J. Intell. Transp. Sys.* **2023**, *4*, 348–359. [CrossRef]
28. Gysen, B.L.J.; Paulides, J.J.H.; Janssen, J.L.G.; Lomonova, E.A. Active Electromagnetic Suspension System for Improved Vehicle Dynamics. *IEEE Trans. Veh. Technol.* **2010**, *59*, 1156–1163. [CrossRef]

29. Papaioannou, G.; Ning, D.H.; Jerrelind, J.; Drugge, L. A K-Seat-Based PID Controller for Active Seat Suspension to Enhance Motion Comfort. *SAE Int. J. Connect. Autom. Veh.* **2022**, *5*, 189–199. [CrossRef]
30. *ISO 2631-1:1997*; Mechanical Vibration and Shock—Evaluation of Human Exposure to Whole-Body Vibration—Part 1: General Requirements. International Organization for Standardization: Geneva, Switzerland, 1997.

Disclaimer/Publisher's Note: The statements, opinions and data contained in all publications are solely those of the individual author(s) and contributor(s) and not of MDPI and/or the editor(s). MDPI and/or the editor(s) disclaim responsibility for any injury to people or property resulting from any ideas, methods, instructions or products referred to in the content.